

# Numerical Simulation and Design of the Air Conditioning System for the 3GeV TPS Electron Storage Ring

J.C. Chang<sup>a</sup>, M.T. Ke<sup>b</sup>, Z.D. Tsai<sup>a</sup>, and J. R. Chen<sup>a</sup>

<sup>a</sup> National Synchrotron Radiation Research Center (NSRRC)

101 Hsin-Ann Rd., Science Park, Hsinchu 30076, Taiwan

<sup>b</sup> Graduate Institute of Air-Conditioning and Refrigeration Engineering, National Taipei University of Technology, Taipei 106, Taiwan

## Abstract

*Having been running the Taiwan Light Source (TLS) for twelve years, National Synchrotron Radiation Research Center (NSRRC), Taiwan has proposed to build a photon source (TPS) in the near future. TPS is preliminarily designed with 3.0 GeV in energy, 518.4m in circumference and 24 Double-Bend Achromat (DBA). Thermal effect is one of the most critical considerations for designing such an advanced accelerator. This research designed the Air Conditioning (AC) system for the TPS and applied Computational Fluid Dynamic (CFD) technique to simulation the air flow and temperature distribution in the storage ring. In the 3-dimensional CFD simulation, vacuum chambers, magnets of the booster and the storage ring, girders and supplied and return wind ducts are modelled. The spatial and temporal temperature variations and air flow were demonstrated through the numerical simulation. The cooling load and capacity of the AC system are estimated. The layouts of Air Handling Units (AHU) and wind ducts has been designed and demonstrated in 3-dimensional drawing.*

## 1. Introduction

It has been more than thirteen years since the first beam stored in the storage ring at TLS. TLS is also known as the first third-generation synchrotron radiation facility in Asia. Although the reliability and stability of the light source have been remarkably upgraded, TLS has gradually lost its advantage of competition due to its limitation straight sections and available space for new insertion devices. Confronting increasing demand for more state-of-the-art researches, the former Board of SRRC had suggested to study the feasibility of constructing another synchrotron light source in February 2001 and Board of NSRRC had decide to propose to construct the TPS to the government in 2004.

Presently, there are more than ten mid-energy synchrotron accelerators around the world in operation or under construction. In such a competitive circumstance, TPS is designed to achieve the targets of low emittance, high brightness, stability and reliability. Each subsystem of the TPS will apply the most advanced and reliable techniques to achieve this goal.

According to the study of utility effects on the beam stability, thermal effect is the most critical mechanical factor affecting the beam stability [1] [2]. Therefore, the design of the AC system of the TPS, especially for the storage ring tunnel, is crucial to affect the beam stability. Our successful experience at TLS will be valuable in designing the AC system of the TPS. One of our analysis tools is the CFD technique. The TLS has applied the CFD technique on the air-cooling magnet lattice girder [3], the experimental hall [4] and the storage ring tunnel [5]. The air temperature variation in the storage ring tunnel is globally controlled within  $\pm 0.1^{\circ}\text{C}$  currently. However, it is believed that a more critical temperature control requirement is needed for the TPS. The new goal of the temperature temporal variation in the storage ring tunnel is targeted at  $\pm 0.02^{\circ}\text{C}$ . Therefore, numerical simulation will be applied again in the AC system of the TPS. Especially in the design phase, there is no physical constructed and no actual experiment conducted yet, numerical simulation becomes a valuable analysis tool.

## 2. Design Concept

AC system may be basically classifiable as 'comfort AC' or 'industrial AC'. NSRRC is equipped with both. In the design of the AC system of TPS, the basic requirements of comfort AC must be met, but industrial AC requires stricter conditions to be satisfied.

### ***Precision Control***

Controlling the temperature in the storage ring tunnel is very important because the ring is where the photon beam and many critical apparatus are located. In particular, the variation of temperature with time must be maintained within  $\pm 0.1$  °C. The AC system at TLS has met this requirement. The new goal of the temperature temporal variation in the TPS storage ring tunnel is targeted at  $\pm 0.02$ °C.

### ***Uniform and Effective Air circulation***

The spatial uniformity of temperature is another important issue in the AC system. The key techniques include the distributions of the air exit and air exhaust, and the controls of the temperature and flow rate. Numerical simulation is a helpful design tool, and has been developed in the NSRRC.

### ***Issue of Vibration and Noise***

The precision of the control of the electron beam is critical, and any vibration of nearby apparatus, especially high-power apparatus, will influence the stability of the beam. The specifications of the anti-vibration devices are particularly important. Several anti-vibration techniques are applied to yield optimal results. Similar strategies will be also applied against noise.

### ***Spatial Configuration***

The AC system typically occupies more space than the other subsystems in the accelerator. It occupies the space of the equipment itself and the space required for maintenance. Therefore, the spatial configuration is another practical issue. Experiences of advanced foreign accelerators and TLS are helpful for reference.

### ***Air Freshness***

Comfort is another important consideration. Particularly in a large experimental hall, ventilation, the filtering device and humidity control are critical.

### ***Power Saving***

An AC system not only requires a large space, but also consumes more power than other subsystems of the accelerator. Hence, saving power is also important.

## **3. AC System Cooling Capacity Estimation and Configuration**

The area of TPS may be estimated to be around  $\pi \times (220^2 - 139^2) / 4 = 22,827$  m<sup>2</sup>. This is approximately 4.5 times the area of the current TLS. The total area of every floor and trench of the TPS is about 33,140m<sup>2</sup>. Accordingly, the cooling capacities of the chiller, the cooling tower and the AHU of the TPS should be more than triple those of the TLS. Therefore, the roughly estimated capacities of the chiller, the cooling tower and the AHU of the TPS are 4000RT, 5000RT and 3000RT, respectively. The storage ring tunnel has 12 AHUs and the experimental hall has about 30 AHUs.

The future TPS will have two underground trenches for technical equipment of some subsystems of the accelerator. Two power substations and AHUs are located in the inner trench (trench A), and the electrical equipment and apparatus for the experimental hall are located in the outer trench (trench B), as presented in Figure 2. The piping system in trench A is mainly for the storage ring tunnel. Trench A is divided into 12 sections. Each section has two AHUs, associated with the AC of the storage ring tunnel and the experimental hall. Trench B has 18 AHUs that serve the AC of the experimental hall and laboratories.

The supply wind duct and the return wind duct for the storage ring tunnel are located on the up and low sides near the inner wall respectively, as shown in the Figure 1. The configuration of the wind ducts is

model in the CFD simulation. The inner supply wind duct and the return wind duct for the experimental hall are installed overhead, as shown in the Figure 1. There is another pair of supply wind duct and the return wind duct for the storage ring tunnel, which is not shown in the Figure 1, also located overhead but on the outer ring of the experimental hall.

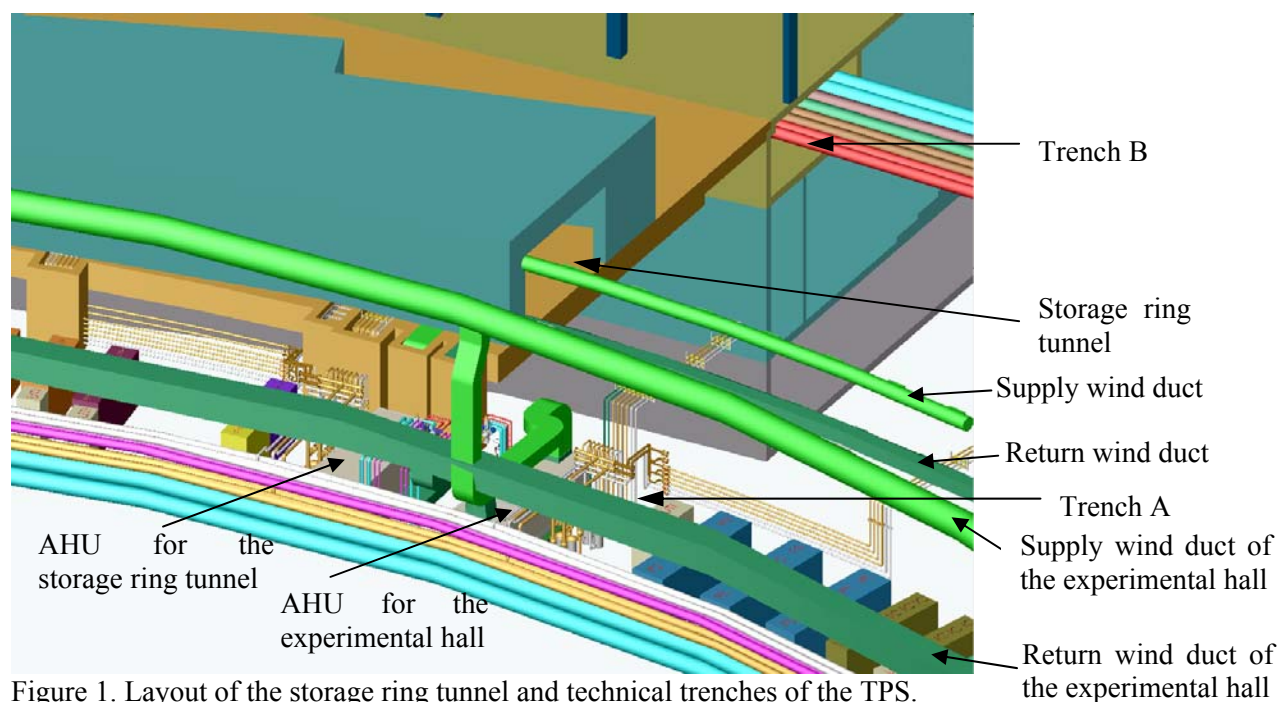


Figure 1. Layout of the storage ring tunnel and technical trenches of the TPS.

#### 4. Numerical Simulation

The temperature distribution and flow fields in the storage ring of TPS are numerically simulated in this study. We use FLUENT 6.2 to perform the numerical simulation. FLUENT is a CFD computer program with complete grid flexibility for modelling fluid flow and heat transfer in complex geometries. FLUENT is composed of three parts, pre-processor, core operation and post-processor. GAMBIT, an integrated pre-processor, is used for geometry modelling and grid generation.

Both steady and transient states are simulated in this study. The simulation of the steady state is used to examine the temperature distribution and the flow field in the whole storage tunnel. The simulation of the transient state is mainly used to check the temperature temporal variation near accelerator equipment.

##### *Model Construction and Grid Generation*

Because the whole space of the storage ring tunnel is too large to simulate and the simulation may consumes too much memory, the geometry modelling is simplified. We divide the storage ring tunnel as periodically symmetric 24 sections and assume periodic boundary condition for each section. Then we simplify the simulation by only simulating one section.

All new designed magnets of the storage ring and booster, girders supplied and return ducts are modelled in the simulation. Two kinds of the supplied air exit and air exhaust are modelled in two cases A and B. The dimension of the air exit and air exhaust in the case A is  $0.5\text{m} \times 0.5\text{m}$ . Both distance between two adjacent air exits and air exhausts are 5 m. In case B, both air exit and air exhaust are modelled as continuous openings with 0.25m in width on the middle of the supplied and return wind ducts, respectively to achieve better spatial uniformity of the temperature distribution. New designed vacuum chambers are also modelled in case B. Figures 2 (A) and (B) demonstrate the physical model and grid structure of the simulation of cases A and B, respectively.

### Governing Equation

The basic governing equations include the continuity equation, the momentum equation and the energy equation. We set our simulated model as a 3D, incompressible and turbulent flow in this study. Both steady-state and transient flows are simulated. We apply the  $k$ - $\varepsilon$  turbulence model and SIMPLEC to solve the velocity and pressure problem.

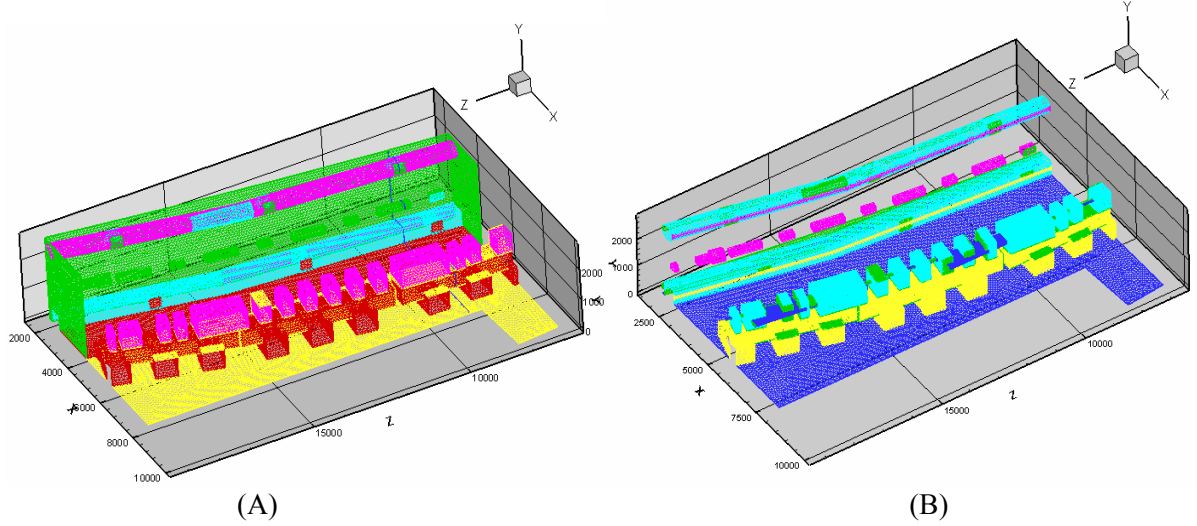


Figure 2 Physical model and grid structure of the simulation of cases A and B.

The basic form of the diffusion equation is

$$\text{div}(\rho\phi v) = \text{div}(\Gamma\nabla\phi) + S_\phi \quad (1)$$

There are different effective diffusion coefficient  $\Gamma_{\phi,eff}$  and source term  $S_\phi$  corresponding to different  $\phi$  in Eq.(1) as shown in Table 1, where the effective molecular viscosity  $\mu_{eff}$  is sum of the turbulent  $\mu_t$  and the laminar viscosity  $\mu$ .

$$\mu_{eff} = \mu_t + \mu \quad (2)$$

Table 1 Effective diffusion coefficient  $\Gamma_{\phi,eff}$  and source term  $S_\phi$  corresponding to different  $\phi$

Equation	$\phi$	$\Gamma_{\phi,eff}$	$S_\phi$
Continuity	1	0	0
Momentum	$U_i$	$\mu_{eff}$	$-\partial p / \partial x_i$
Energy	$T$	$k_{eff}$	S (cooling load)
Turbulence kinetic energy	k	$\mu_{eff} / \sigma_k$	$\frac{P_k - \rho\varepsilon}{k} + G_k$
Turbulence kinetic energy dissipation rate	$\varepsilon$	$\mu_{eff} / \sigma_\varepsilon$	$\frac{\varepsilon(C_1 P_k - C_2 \varepsilon)}{k} + \frac{C_3 G_k \varepsilon}{k}$

where  $\Gamma_{\phi,eff}$  is the effective diffusion coefficient,  $S_\phi$  is the source term,  $P_k = \mu_t (u_{i,j} + u_{j,i})u_{i,j}$ ,  $\mu_t = C_\mu \rho k^2 / \varepsilon$ ,  $\sigma_k = 1.0$ ,  $\sigma_\varepsilon = 1.314$ ,  $\sigma_c = 1.0$ ,  $C_1 = 1.44$ ,  $C_2 = 1.92$ ,  $C_3 = 1.0$ ,  $C_\mu = 0.09$ . According to the mass conservation,  $\phi = 1$ ,  $\Gamma_{\phi,eff} = 0$  and  $S_\phi = 0$  are substituted into Eq.(1) to obtain the continuity equation

$$\frac{\partial \rho}{\partial t} + \rho \left[ \frac{\partial u}{\partial x} + \frac{\partial v}{\partial y} + \frac{\partial w}{\partial z} \right] = 0 \quad (3)$$

where  $\rho$  is the fluid density,  $u$ ,  $v$  and  $w$  are velocities of x, y and z directions, respectively.

According to the momentum conservation,  $\phi$ ,  $\Gamma_{\phi,eff}$  and  $S_{\phi}$  are substituted into Eq.(1) to obtain the momentum equation. Here we only show the momentum equation in x direction. In x direction we have  $\phi = u$ ,  $\Gamma_{\phi,eff} = \mu_{eff}$  and

$$S_{\phi} = -\frac{\partial P}{\partial x} + \frac{\partial}{\partial x} \left( \mu_t \frac{\partial u}{\partial x} \right) + \frac{\partial}{\partial y} \left( \mu_t \frac{\partial v}{\partial x} \right) + \frac{\partial}{\partial z} \left( \mu_t \frac{\partial w}{\partial x} \right) \quad \text{to obtain the}$$

momentum equation in x direction as follows.

$$\begin{aligned} \frac{\partial(\rho u)}{\partial t} + \frac{\partial(\rho u u)}{\partial x} + \frac{\partial(\rho v u)}{\partial y} + \frac{\partial(\rho w u)}{\partial z} &= \frac{\partial}{\partial x} \left( \mu \frac{\partial u}{\partial x} \right) + \frac{\partial}{\partial y} \left( \mu \frac{\partial u}{\partial y} \right) + \frac{\partial}{\partial z} \left( \mu \frac{\partial u}{\partial z} \right) \\ &\quad - \frac{\partial P}{\partial x} + \frac{\partial}{\partial x} \left( \mu_t \frac{\partial u}{\partial x} \right) + \frac{\partial}{\partial y} \left( \mu_t \frac{\partial v}{\partial x} \right) + \frac{\partial}{\partial z} \left( \mu_t \frac{\partial w}{\partial x} \right) \end{aligned} \quad (4)$$

Likewise, according to energy conservation,  $\phi = T$ ,  $\Gamma_{\phi,eff} = k$  and  $S_{\phi} = S =$  heat source, are substituted into Eq.(1) to obtain the energy equation as follows.

$$\left( \frac{\partial T}{\partial t} + u \frac{\partial T}{\partial x} + v \frac{\partial T}{\partial y} + w \frac{\partial T}{\partial z} \right) = \alpha \left( \frac{\partial^2 T}{\partial x^2} + \frac{\partial^2 T}{\partial y^2} + \frac{\partial^2 T}{\partial z^2} \right) + S \quad (5)$$

### Boundary Condition

Boundary conditions are assumed according to designed data of each subsystem. The air velocity at each air exit is 5 m/s and ratio of velocity in X direction to Y direction is 2/-1. The air temperature at each air exits is set as 20 °C. All magnets of the booster and the storage ring and vacuum chambers are heat sources. All girders, walls, the ceiling and the floor are assumed adiabatic. Boundary conditions in cases A and B are the same. The detailed boundary conditions are list in Table 2.

Table 2 Boundary conditions for the CFD simulation.

Air exit	Air velocity	5.0 m/s (X/Y ration = 2/-1)
	Temperature	20.0 °C
Magnets of the storage ring		2.0 W/m <sup>3</sup>
Magnets of the booster		1.5 W/m <sup>3</sup>
Vacuum chamber		2.0 W/m <sup>3</sup>
Girder, ceiling, wall and floor		Adiabatic

### Convergence Criterion

Because of the truncation error of the numerical computation and the differences of computed values resulted from the iteration, there exists small difference between two sides of the governing equation. This difference is known as the residual value. The residual value is used as the index of the convergence criterion in the numerical simulation. All the residual values of all physical parameters are set as  $1 \times 10^{-6}$ . If the residual value is not larger than  $1 \times 10^{-6}$ , the iteration is considered convergent.

## 5. Results and Discussion

In order to compare the effects of the layout of air exit and exhaust to the temperature distribution and the flow field, we simulated two cases with different layouts of air exit and exhaust in this study. The physical model and grid structure of both cases are shown in Figure 2.

Figure 3 shows the simulated steady state temperature field of case A.. Two planes A and B of Z direction are created to check the simulated results, as shown in the figure. Plane A is located at one air exit while plain B is located at one air exhaust. The temperature field on plane A clearly illustrates one band zone of temperature = 20~21 °C in blue color. This zone starts from the air exit and its orientation matches the flow direction. This phenomenon disappears in plane B. On the contrary, a zone of temperature = 23~ 24 °C forms near the air exhaust. All magnets in Figure 3 show various color whose temperature ranges from 24 °C to 29 °C. The temperature on both sides of most magnets is lower than temperature on the top of the magnet.

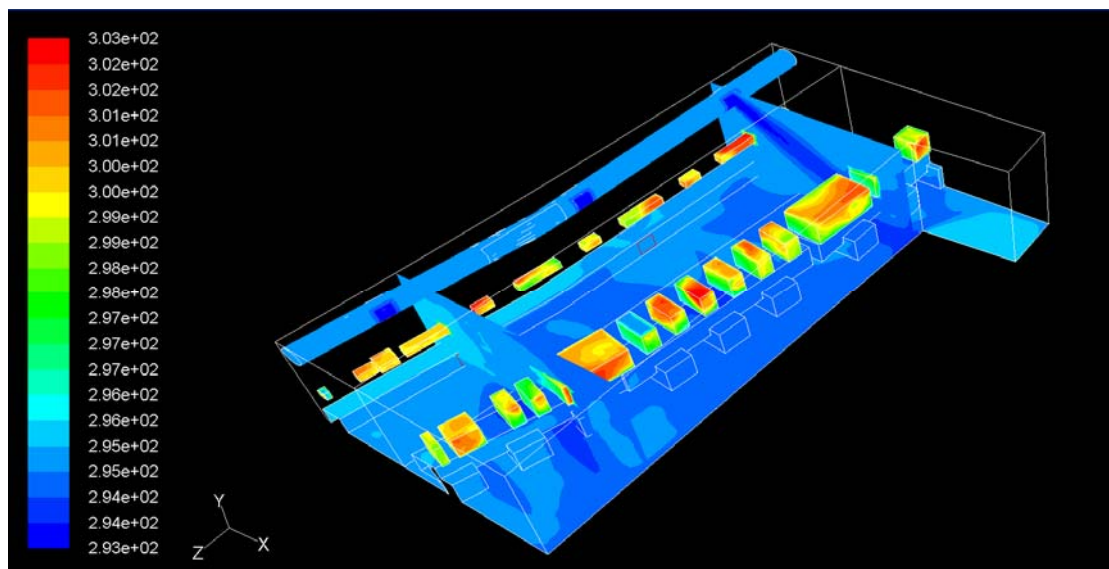


Figure 3 Simulated temperature field of case A.

Figure 4 shows the simulated steady state flow field of case A.. It shows higher flow velocity on the plane A than that on the plane B. The flow direction on the plane A clearly matches with mentioned band zone in Figure 3. On the plane B, only few streamlines are observed near the air exhaust and the magnet.

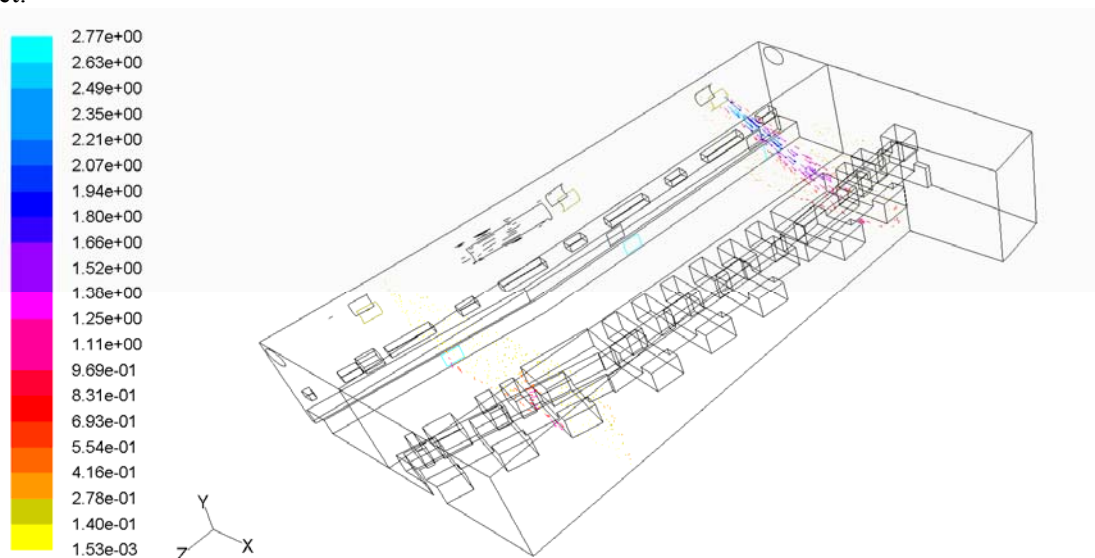


Figure 4 Simulated flow field of case A.

Figure 5 shows the simulated steady state temperature field of case B. The temperature fields on both planes A and B are similar because of the continuous air exit and exhaust. A zone of low temperature is

clearly illustrates near the air exit on both planes A and B. The continuous band zone on the supply air duct also show low temperature in blue color. The temperature of all magnets and vacuum chambers ranges from 27 °C to 28 °C, which is more uniform than that in Figure 3. The temperature of this result verifies that the design of air exit and exhaust of case B can achieve better thermal uniformity than that of case A.

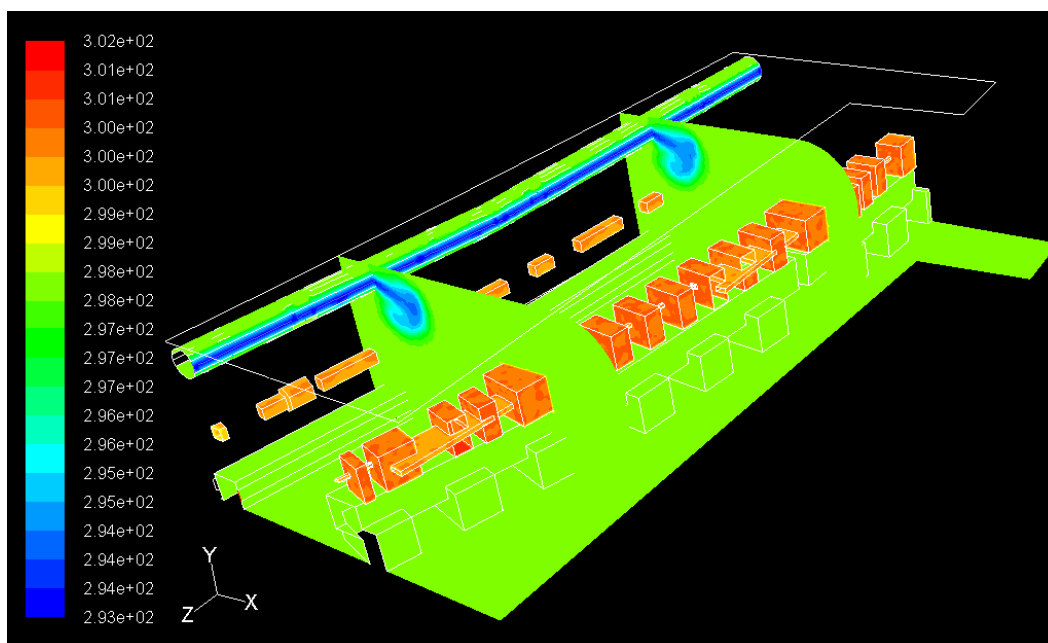


Figure 5 Simulated temperature field of case B.

Figure 6 shows the simulated steady state flow field of case B. Likewise, similar flow field forms on planes A and B. The flow velocity at the exit is higher than that of other location. The return flow near the air exhaust is also clearly illustrated.

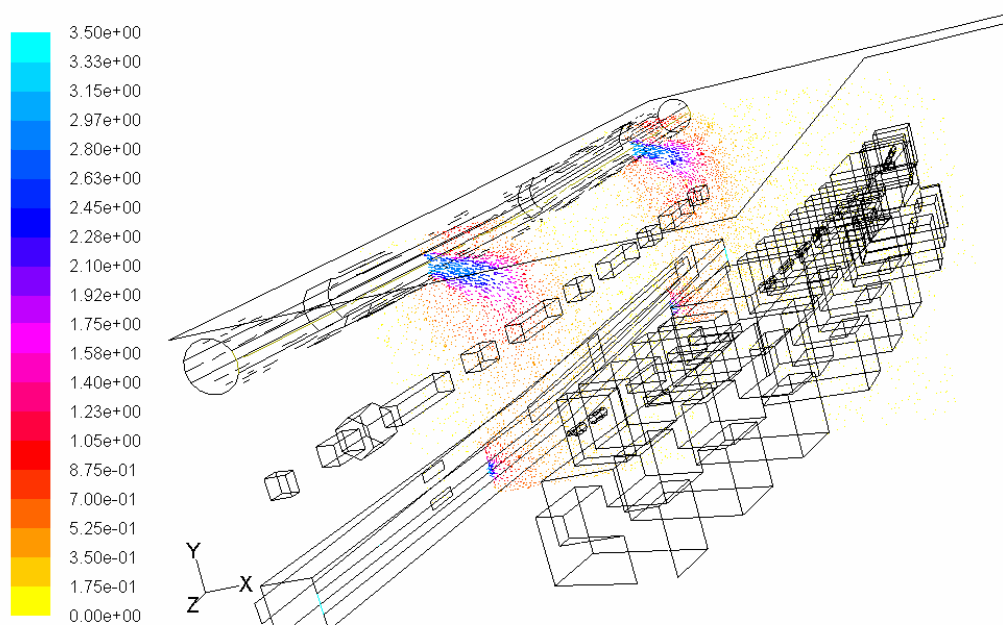


Figure 6 Simulated flow field of case B.

In order to simulate the transient state of the temperature field, boundary conditions of some heat sources list in Table 2 are modified and list in Table 3. We also select eight points respectively above

magnets of the booster and the storage ring 10cm or 20cm to examine simulated temperature temporal variations. The simulated results show that the temperatures temporal variations vary from  $\pm 0.023$  °C to  $\pm 0.007$  °C. The simulated results of the temperature variations are list in Table 4.

Table 3: Boundary conditions for the CFD transient simulation.

Magnets of the storage ring	$2.0 + 0.2\cos(0.1t) \text{ W/m}^3$
Magnets of the booster	$1.5 + 0.15\cos(0.1t) \text{ W/m}^3$
Vacuum chamber	$2.0 + 0.2\cos(0.1t) \text{ W/m}^3$

Table 4: Simulated temperature temporal variation.

No.	Location	Temperature variation
1	Above the 1st dipole magnet of the ring 10 cm	$\pm 0.023$ °C
2	Above the 1st dipole magnet of the ring 20 cm	$\pm 0.013$ °C
3	Above the 2nd dipole magnet of the ring 10 cm	$\pm 0.021$ °C
4	Above the 2nd dipole magnet of the ring 20 cm	$\pm 0.011$ °C
5	Above the middle quadrupole magnet of the ring 10 cm	$\pm 0.017$ °C
6	Above the middle quadrupole magnet of the ring 20 cm	$\pm 0.009$ °C
7	Above the one sextupole magnet of the booster 10 cm	$\pm 0.014$ °C
8	Above the one sextupole magnet of the booster 20 cm	$\pm 0.007$ °C

## 6. Conclusion Remarks

The cooling capacity of the AC system of the TPS was estimated, and the cooling capacities of the chiller, the cooling tower and the AHU of the TPS are about 4000RT, 5000RT and 3000RT, respectively. The configuration of the AC system was also designed. Twenty four and eighteen AHUs were designed to be installed trenches A and B for the storage ring tunnel and the experimental hall, respectively.

The CFD technique was applied to simulate the temperature distribution and the flow field of both steady and transient states of the storage ring tunnel. The simulated results of the steady state show that the design of continuous air exit and exhaust of case B can achieve better thermal uniformity than that of case A. Eight points respectively above magnets of the booster and the storage ring 10cm or 20cm was chosen to examine simulated temperature temporal variations. The simulated of the transient steady results show that the temperatures temporal variations vary from  $\pm 0.023$  °C to  $\pm 0.007$  °C.

## 7. Acknowledgement

The authors would like to thank the colleagues of the utility group of NSRRC for their assistance.

## References

- [1] J.R. Chen, H.M. Cheng, Z.D. Tsai, C.R. Chen, T.F. Lin, G.Y. Hsiung, and Y.S. Hong, "The Correlation between the Beam Orbit stability and the Utilities at SRRC", Proc. of 6th European Particle and Accelerator Conference EPAC98, Stockholm, Sweden, June 22-26, 1998.
- [2] J.R. Chen, D.J. Wang, Z.D. Tsai, C.K. Kian, S.C. Ho, and J.C. Chang, "Mechanical Stability Studies at the Taiwan Light Source", 2nd Int'l Workshop on Mechanical Engineering Design of Synchrotron Radiation Equipment and Instrumentation (MEDSI02), APS, U.S.A., Sep 5-6, 2002.
- [3] D.S. Lee, Z.D. Tsai, J.R. Chen and C. R. Chen, "Cooling Air Flow Induced Thermal Deformation of the Magnet Lattice Girder", Proceedings of European Particle Accelerator Conference EPAC2000, Vienna, Austria, June 26-30, 2000.
- [4] J.C. Chang, M. T. Ke, C.Y. Liu, and J.R. Chen, "Air Temperature Analysis and Control Improvement for the Large-Scale Experimental Hall" 2004 Asian Particle and Accelerator Conference (APAC), March 22-26, 2004, Gyeongju, Korea.
- [5] J.C. Chang, J.R. Chen, Z.D. Tsai and M. T. Ke "Air Temperature Analysis and Control Improvement for the Storage Ring Tunnel" 2005 Particle and Accelerator Conference (PAC), May 16-20, 2005, Knoxville, USA.